Robotica (2013) volume 31, pp. 955–968. © Cambridge University Press 2013
doi:10.1017/S0263574713000209

Biomimetic-based output feedback for attitude stabilization of a flapping-wing micro aerial vehicle

H. Rifaï†*, J.-F. Guerrero-Castellanos‡, N. Marchand§ and G. Poulin-Vittrant¶

† *LISSI, 120-122 rue Paul Armangot, 94400 Vitry-Sur-Seine, France*
‡ *Faculty of Electronics, Autonomous University of Puebla (BUAP), Puebla, Mexico*
§*GIPSA Lab, Control Systems Department, ENSE3/CNRS, Saint Martin d'Hères, France*
¶*Greman, UMR 7347 CNRS, University François Rabelais de Tours, Site de Blois, Rue de la Chocolaterie, 41000 Blois, France*

(Accepted February 24, 2013. First published online: April 10, 2013)

SUMMARY
The paper deals with the development of a bounded control law for Flapping-wing Micro Aerial Vehicles that mimics a strategy adopted by animal flapping flyers to stabilize their orientation. The control consists on generating torques about the body's principal axes by means of a modulation of the wing angle amplitudes. It is known that flapping flyers orient their body without any numerical computation or estimation of their current attitude. Therefore, the proposed control law is computed using the direct measurements of onboard sensors mimicking animal sensitive organs, more specifically the halteres, legs sensilla, and magnetic sense. The technological equivalents of these biological sensors are three rate gyros, a tri-axis accelerometer, and a tri-axis magnetometer, respectively. Besides, the control signal is bounded to keep the wing angle amplitudes below the maximal values. Owing to its simplicity, this control law is suitable for applications where onboard computational resources are limited. The stability of the closed-loop system is proved based on Lyapunov analysis and averaging theory. The effectiveness of the proposed control law is shown in simulations. The robustness with respect to external disturbances is also shown emphasizing the importance and need of the bounded control.

KEYWORDS: Aerial robotics; Biomimetic robots; Control of robotic systems; Bounded control; Micro robotics.

1. Introduction
Animal flapping flyers depict several techniques to achieve flight and maneuvers moving their wings, body, and legs.[16] Principally, these techniques get benefit of the wing morphology, aerodynamic effects, sensory and actuating systems, flight control, and obstacle avoidance mechanisms. For example, insects are able to change, very quickly, their speed and direction of flight, within almost 100 ms especially during predatory phases.[16] They are also able to accomplish a transitory lateral or backward flight. These maneuvers are performed by a displacement of the abdomen or an asymmetrical evolution of the wings using an amplitude modulation[1,27] or phase modulation,[26] and frequency modulation occurs very rarely.[27]

Besides, the flapping flyer is endowed with information, issued from multiple sensitive organs, about its state, interaction with the environment as well as local destination to determine the way to reach it. For insects, one can cite the ocelli, the compound eyes, and other biological sensors detailed as follows[2,4,16] (and references therein):

- Halteres are gyroscopic biological sensors, present at the wing bases, that detect the rotational movement of the body and allow to determine its angular velocity along the three axes.
- Sensilla are cuticular sense hair detecting chemical or mechanical stimuli. They are present on the antenna, wings, and legs. Legs sensilla, for example, allow to determine the direction of the gravity field with respect to the insect's body.
- Magnetic sense allows to determine the direction of the earth magnetic field with respect to the insect's body.

Using a fusion of information issued from these organs, the insect determines its trajectory and adapts its body's velocity and orientation to track it. One should emphasize that these actions are executed by the insect without any instantaneous numerical knowledge of its position, orientation, or velocity.

Insect's performance has encouraged the design of Flapping-wing Micro Aerial Vehicles (FMAVs). The micro aerial vehicle is a small-size aircraft, having a maximal dimension of 6 inches,[1] and intended to perform an autonomous flight, thanks to an onboard control system, comprising a set of sensors and dedicated integrated circuits. Due to their small size and flapping movement, FMAVs fly in zones characterized by low Reynolds numbers (10^2–10^4). They develop, therefore, extra nonstationary aerodynamic

* Corresponding author. E-mail: hala.rifai@u-pec.fr
The paper lies within the scope of the project OVMI/EVA sponsored by the French National Research Agency.

[1] The definition is given by the DARPA (Defense Advanced Research Projects Agency).

forces, which help them reduce the forces generated by the actuators to accomplish the flight and, consequently, reduce the energetic consumption. The FMAVs produce low noise. They are able to accomplish vertical taking-off and landing as well as stationary flight in hovering mode. However, their major drawback is still the difficulty of identifying and implementing the complex mechanisms carried out by insects to perform maneuvers.[16,20] The FMAVs are intended for use in areas inaccessible for people or that require high accuracy of intervention.

The present paper deals with the modeling and attitude stabilization of an FMAV for scenarios necessitating to maintain a stable orientation in front of a scene in order to monitor or investigate it. A simple model mimicking the flapping flight is presented, including the wing's degrees of freedom, the sensorimotor system, as well as the developed aerodynamic forces. The major contribution of this work is the development of a biomimetically inspired control strategy aiming to stabilize the orientation of the FMAV. The inputs of the control law are the direct measurements of onboard sensors, equivalent to those which an insect is equipped with, without the need of an explicit attitude reconstruction (represented by the Euler angles in $\mathbb{R}^3$, quaternion in $\mathbb{S}^3 \subset \mathbb{R}^4$, or rotation matrix in $SO(3)$). Hence, unlike conventional approaches, the computational cost used for the attitude estimation/reconstruction is avoided. Note that attitude estimation is frequently carried out by means of extended Kalman filters or nonlinear observers, which represent a high computational cost. The control law takes into consideration the wing angle amplitude bounds, characterizing the animal species. It has the easiness of a Proportional Derivative (PD) controller, the derivative term is obtained by means of the halteres (angular velocity) and the proportional term by means of legs sensilla and magnetic sense (direct measurement of attitude error). Moreover, the control is very simple and therefore is suitable to be implemented in real time. It is also independent of the FMAV body's inertia, modeling or aerodynamic errors, and robust with respect to external disturbances. Unlike fuzzy logic controllers or fractional Proportional Integral Derivative (PID) controllers, the bounds of the control signal are taken into account explicitly and the stability properties are well established.

Models of FMAVs existing in the literature consider them as rigid bodies subject to external forces and torques generated by the flapping wings whose amplitude and/or phase may be modulated[9,10,12,29,31] phased or even both of them.[9,10,29] Few works have treated the problem of controlling the orientation of flapping aerial vehicles based on sensor measurements. A proportional derivative output feedback based on ocelli and halteres measurements has been proposed[36]. Another work has considered a linear quadratic optimal control based on ocelli, magnetic compass and halteres measurements[11,14]. Halteres measurements have also been used to estimate the pitch rate and stabilize the corresponding angle with a proportional derivative controller and pole placement[7]. Rate gyros, accelerometer and magnetometer sensors, representing respectively the halteres, legs sensilla and magnetic compass have been used to estimate the insect's attitude (rotation matrix), used after, along with angular velocity measurement, in a state feedback control law[4]. One should emphasize that, in the aforementioned works, the proposed linear control laws cannot be sufficiently robust with respect to external disturbances representing wind, for example. Note also that building a control law using estimated attitude state is not a biomimetic approach. In fact, insects have no numerical instantaneous determined orientation knowledge (angles or rotation matrix) but only information issued directly from their biological sensors.[6]

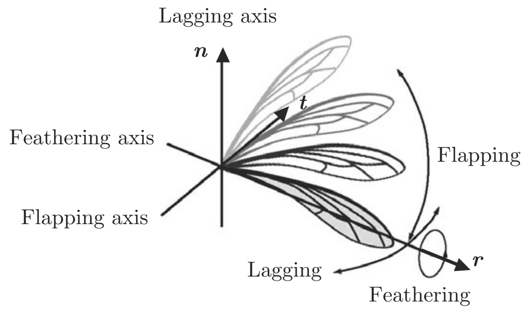

Fig. 1. Degrees of freedom of a wing: flapping, lagging (elevation), and feathering.

The paper is organized as follows. In Section 2, the model of the FMAV is proposed in agreement with insect models, including the sensorimotor systems, aerodynamic forces, and body's dynamics. A biologically inspired bounded control law, based directly on the measurements of some embedded sensors and aiming to stabilize the orientation of the FMAV, is presented in Section 3. Simulation results are addressed in Section 4 as well as some robustness tests. Finally, conclusions are given in Section 5 and future works are introduced.

2. Insect Flight Versus Biomimetic Robot Flight

The present section deals with the design and modeling of an FMAV. Design concerns mainly the choice of the sensors and actuators to embark on the FMAV. Therefore, the insect's sensorimotor system is shortly presented and correlated to the technological corresponding equipments. Modeling concerns principally the establishment of a simple mathematical model allowing to represent the degrees of freedom of the flapping flight as well as aerodynamic forces and mechanisms deployed by nature's flapping flyers to perform maneuvers. One should note that a beating wing is in interaction with the surrounding airflow, which creates aerodynamic forces perpendicular to its surface. These forces generate the linear and rotational movements of the FMAV's body.

2.1. Wing degrees of freedom

The movement of a wing is a combination of several elementary actions:[6,40] flapping, feathering, lagging, or elevation besides flexion and torsion (Figs. 1 and 2). Flapping is an up-and-down movement of the wing represented by a rotation of the wing about its tangential axis $\boldsymbol{t}$ of a flapping angle ϕ. Feathering is a rotation of the wing about its

https://doi.org/10.1017/S0263574713000209 Published online by Cambridge University Press

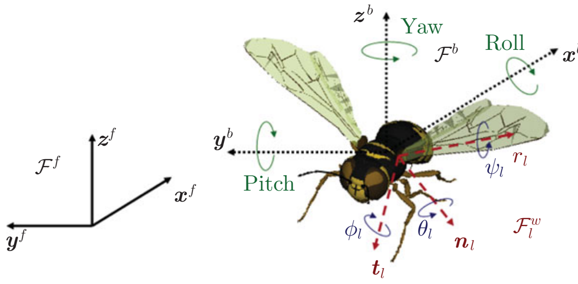

Fig. 2. (Colour online) Coordinate frames: inertial fixed frame $\mathcal{F}^f(\boldsymbol{x}^f, \boldsymbol{y}^f, \boldsymbol{z}^f)$, body attached frame $\mathcal{F}^b(\boldsymbol{x}^b, \boldsymbol{y}^b, \boldsymbol{z}^b)$, and left wing attached frame $\mathcal{F}_l^w(\boldsymbol{r}_l, \boldsymbol{t}_l, \boldsymbol{n}_l)$.

spanwise axis $\boldsymbol{r}$ of a rotation angle ψ. Lagging or elevation is a forward–backward movement of the wing parallel to the body, modeled by a rotation about a normal axis $\boldsymbol{n}$ of a deviation or elevation angle θ. Flexibility of the wing allows it to resist to turbulence, provides a gentler flight, and increases the aerodynamic force relative to a same size rigid wing.[13] Torsion is a twist movement of the wing, providing an aerodynamic stability.[37]

The directions of the wing rotational axes are chosen such that $\boldsymbol{r}$ is oriented from the wing base to its tip along the wingspan, $\boldsymbol{t}$ is parallel to the wing chord, oriented from trailing to leading edge, and $\boldsymbol{n}$ is perpendicular to the wing plane-oriented, so that the three-sided frame $\mathcal{F}^w(\boldsymbol{r}, t, n)$ is direct. Note that the frame $\mathcal{F}^w$ should be indexed, left $\mathcal{F}_l^w$ and right $\mathcal{F}_r^w$, relative to the left and right wings, respectively.

Maneuvers of animal flapping flyers are performed primarily by asymmetrical movements of the wings, a displacement of the abdomen and legs. The movement of the wings generates aerodynamic forces, which resultant is perpendicular to the wing surface. Therefore, the flapping/rotation movements of the wings generate the vertical/longitudinal movements of the insect, respectively. A difference in the amplitudes of the left and right flapping/rotation angles allows to generate a roll/yaw movements, respectively (Fig. 2). The pitch movement can be created by controlling the wing's elevation degree of freedom, or by changing the center of gravity of the body tilting it upward or downward. The second solution allows to reduce the number of embarked actuators and therefore is adopted in the sequel. Finally, the lateral movement is generated by coupling the body vertical lift force with the roll angle, maneuver performed by many birds and insect species.[16]

The wing angles are characterized by their maximal amplitudes and their wingbeat frequency within their predefined trajectory. These values are specific to each species. Generally, flapping-wing flying creatures move their wings according to a sine function with higher harmonics, the fundamental frequency is equal to the wingbeat frequency.[16] A wingbeat period is divided into two phases: the downward phase of the flapping movement or downstroke and, the upward phase or upstroke.[6,16] During downstroke, the flapping flyer orients the dorsal side of the wing to the flow. It orients the ventral side during the upstroke. The model proposed in this work considers the wing as a rigid body, flapping in the mean stroke plane, defined by taking the deviation angle θ to zero. This choice is motivated by the possibility to control insects using only two wing angles.[24] Flapping and rotation angles, ϕ and ψ, are assumed to vary according to saw tooth and pulse functions, respectively, such that the wing changes its orientation at the end of each half stroke (Fig. 3). The time variation of the wing angles is given by Eq. (1):

$$\begin{aligned} \phi(t) &= \begin{cases} \phi_0(1 - \frac{2t}{\kappa T}) & 0 \le t \le \kappa T \\ \phi_0(2\frac{t-\kappa T}{(1-\kappa)T} - 1) & \kappa T < t \le T \end{cases} \\ \psi(t) &= \psi_0 \ \mathrm{sign}(\kappa T - t) \quad 0 \le t \le T \\ \theta(t) &= 0 \qquad\qquad\qquad\quad 0 \le t \le T, \end{aligned} \tag{1}$$

where "sign" designates the classical sign function, T is the wingbeat period, κ is the ratio of downstroke duration to the wingbeat period and should verify $0 < \kappa < 0.5$ to produce a positive aerodynamic lift force over a wingbeat period, ϕ_0 and ψ_0 are, respectively, the amplitudes of flapping and rotation angles. ϕ_0 and ψ_0, considered for left and right wings, will define the control inputs as will be shown in Section 2.6 . This choice is motivated by the fact that wingbeats have generally fixed frequency, except during some maneuver phases. Turns can be created by asymmetrically changing the left and right wing angle amplitudes.[1,27]

Note that the wingbeat frequency has been taken equal to 100 Hz considering in the following the model of a diptera insect.[16] Note also that the given angle parameterization does not represent the real movement of the wings, but the desired trajectory to be achieved by the wing actuators.

Remark 1. The wing angle parameterization adopted in the present work is not unique. Other parameterizations can be used as well. The only condition is that they allow the generation of an aerodynamic body lift force that, averaged over a wingbeat period, should be positive and able to balance the FMAV's weight. The control strategy and control law proposed in the following remain always applicable.

Other non-symmetric wing-parameterizations have been proposed in the literature as the modulation of all three angles.[9] However, embarking many actuators is weight costly. Therefore, strategies have been oriented to decrease their number to two besides a bobweight actuator in the body.[28] Then, the bobweight has been removed and the wings parametrization adapted to use only one actuator per wing.[29] This configuration necessitates the development of complex control laws to stabilize the translational and rotational movement of the FMAV. Other strategies have used one principal and two secondary actuators to accomplish an asymmetric control of the wing angle amplitudes.[18] Another work has considered one active and one passive degrees of freedom allowing to control four wing angles, the aim is to ensure the vertical flight, the orientation, notably the roll and yaw angles, is passively regulated.[38]

https://doi.org/10.1017/S0263574713000209 Published online by Cambridge University Press

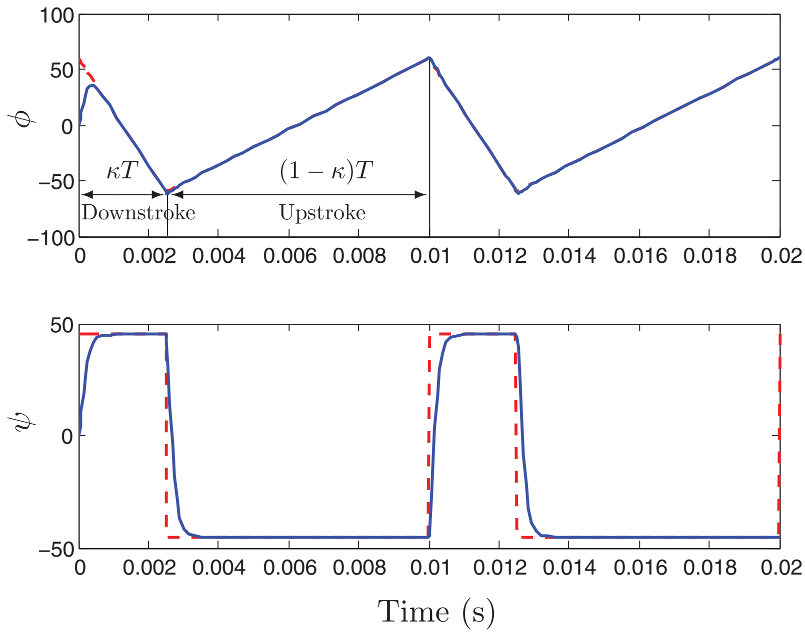

Fig. 3. (Colour online) Shape of the wing angle evolution through an illustrative example: the flapping (top) and rotation (bottom) wing angles, the reference angles in dashed red line, and the real angles (delivered by the actuators) in continuous blue line.

2.2. *Actuation*

The periodic wingbeats are accomplished by the muscles, present at the wing bases or in the thorax and, vibrating with a fixed frequency. This movement can be identified as a vibration at the undamped natural frequency. Therefore, piezoelectric actuators are the most suitable for this application. The reverse effect of piezoelectricity, consisting on applying voltage and retrieving mechanical movement, is of interest. The alternative voltage is delivered by an electronic converter designed specifically for piezoelectric actuators. These actuators behave as reactive loads[5,21] introducing some nonlinearities (hysteresis, creep) that can be avoided using a local control.[23] The controller inputs are the reference angles defined in Eq. (1). The local controller–actuator closed loop is regulated to behave as a first-order filter having fast dynamics, so that the influence of the actuator on the global system dynamics is despised (Fig. 3):

$$\ddot{A} = \ddot{A}_r - \lambda_1(\dot{A} - \dot{A}_r) - \lambda_2(A - A_r), \qquad (2)$$

where A is the amplitude of the flapping or rotation angles at the actuator's output and A_r is the reference amplitude at the actuator's input. λ_1 and λ_2 are computed using pole placement such that the time constant of the local closed-loop is equal to $\tau = 0.1$ ms: $\lambda_1 = \frac{2}{\tau}$ and $\lambda_2 = \frac{1}{\tau^2}$.

Remark 2. Note that the piezoelectric actuators available on the market have very fast dynamics with a time response reaching the microsecond range (PZT, piezoceramic actuators, for example). The conservative hypothesis considered for $\tau = 0.1$ ms is, therefore, absolutely realistic even when the actuator is coupled to the wing. Note that if the time response of the wing–actuator system is less than 0.1 *ms*, it will be more advantageous for the transparency of the actuator and its influence on the FMAV's movement.

2.3. *Sensory system*

In attitude stabilization theory, the FMAV's body should reach a desired orientation and maintain it, which means that, at stationary hovering flight, the body axes should be aligned to some reference axes with a null angular velocity. Within insect biosensors, the halteres, legs sensilla, and magnetic sense contribute to control the body's orientation. These sensitive organs have some technological equivalents, respectively, the rate gyros, accelerometers, and magnetometers.

Define a fixed frame in the space $\mathcal{F}^f(\boldsymbol{x}^f, \boldsymbol{y}^f, \boldsymbol{z}^f)$ and a mobile frame attached to the FMAV's body at its center of gravity $\mathcal{F}^b(\boldsymbol{x}^b, \boldsymbol{y}^b, \boldsymbol{z}^b)$ (indexes, f and b, stand for fixed and body, respectively) (Fig. 2). Define also a rotation matrix $R \in SO(3) = \{R \in \mathbb{R}^{3\times 3} : R^T R = I_3, \det R = 1\}$ allowing the transformation from the fixed frame $\mathcal{F}^f$ to the body frame $\mathcal{F}^b$.

2.3.1. *Rate gyros.*

Three rate gyros are mounted orthogonally on the FMAV's body such that their axes coincide with the body's axes. The sensors deliver the angular velocity measurements about the body's axes. The measured angular velocity, ω_G, is given by:

$$\omega_G = \omega + \xi_G, \qquad (3)$$

where $\omega \in \mathbb{R}^3$ is the angular velocity of the body and $\xi_G \in \mathbb{R}^3$ is a white Gaussian noise of the rate gyros.

2.3.2. *Magnetometer.*

A tri-axis magnetometer is mounted on the FMAV such that its axes coincide with the body's axes. The sensor gives the measurement of the fixed magnetic field in $\mathcal{F}^b$:

$$s_M^b = R\, s_M^f + \xi_M, \qquad (4)$$

https://doi.org/10.1017/S0263574713000209 Published online by Cambridge University Press

where $s_M^f \in \mathbb{R}^3$ is the magnetic field in the fixed frame $\mathcal{F}^f$, R is the rotation matrix from the fixed frame $\mathcal{F}^f$ to the body's frame $\mathcal{F}^b$, and $\xi_M \in \mathbb{R}^3$ is a vector of Gaussian white noise. Note that the magnetic field in the fixed frame is considered constant and equal to $s_M^f = [\frac{1}{2}, 0, -\frac{\sqrt{3}}{2}]^T$ in the geographic zone where the simulations are performed.

2.3.3. Accelerometer. A tri-axis accelerometer is mounted on the FMAV such that its axes coincide with the body's axes. The sensor measures the FMAV's acceleration in $\mathcal{F}^b$. It is given by:

$$s_A^b = R\, s_A^f + \xi_A,$$

where $s_A^f = (a - g e_3)$ with $e_3 = [0, 0, 1]^T$, $g \in \mathbb{R}$ and $a \in \mathbb{R}^3$ are, respectively, the gravity and body's acceleration vectors expressed in the fixed frame $\mathcal{F}^f$. $R \in \mathbb{R}^{3\times 3}$ is the rotation matrix from the fixed frame $\mathcal{F}^f$ to the body frame $\mathcal{F}^b$. $\xi_A \in \mathbb{R}^3$ is a Gaussian white noise. Considering that the FMAV moves at low accelerations such that $\|a\| \ll \|g\|$ and normalizing, the accelerometer measurement is given by:

$$s_A^b = R\, g_n + \xi_A \tag{5}$$

with $g_n = s_A^f = [0, 0, -1]^T$, the normalized gravity vector.

Remark 3. The FMAV experiments acceleration along the body-fixed direction z^b for the taking-off, landing, and translational horizontal movements. Because, in the present work, only the attitude stabilization is considered, the assumption $\|a\| \ll \|g\|$ holds and the tri-axis accelerometer can be used as a reference vector sensor. The gravity vector is the reference vector and the acceleration is considered as a disturbance. If the translational movement has to be considered, a compensation of the vertical acceleration should be envisaged.

2.4. Aerodynamics

The flapping movement of the wings within a surrounding steady airflow generates quasi-steady aerodynamic forces: a lift force, perpendicular to the wing, enhancing the flight and a drag force, parallel and opposing to the airflow.[16] Drag forces generated by the wings are neglected in the present work considering that the wings are made of materials having a sufficiently small friction coefficient and that the drag is generated only by the body.[16] In addition to the quasi-steady aerodynamic forces, the flapping flyer is subject to unsteady aerodynamic forces generated by the rotation of the wing about its radial axis $\boldsymbol{r}$. This rotation creates vortices, adding airflow to the following wingbeats, and creating additional forces. These forces allow the flapping-wing animal to ensure maneuvers such as quick variations of velocity or flight direction and instantaneous turns. All forces are considered applied at the wing's center of pressure, located at l_r equal to 65% of the wing length L from the wing base ($l_r = 0.65\, L$) and at l_t equal to 25% of the chord length C_h from the leading edge ($l_t = 0.25\, C_h$).[35] The center of pressure is considered belonging to the radial axis $\boldsymbol{r}$, given in the wing frame $\mathcal{F}^w$ by $p^w = [l_r, 0, 0]^T$.

2.4.1. Quasi-steady aerodynamic force. The quasi-steady force is generated by the pressure of the airflow exerted on the wing surface. This force is perpendicular to the wing and is applied at the wing's center of pressure. It is oriented to the opposite direction of the wing's velocity. The magnitude of this force is given by:

$$f_{qs} = -\frac{1}{2}\rho C_w S_w v^w |v^w| \tag{6}$$

where ρ is the air density, S_w is the wing surface and v^w is the wing velocity. C_w is the aerodynamic coefficient of the wing. $C_w = C(1 + C_f)$ during downstroke and $C_w = C(1 - C_f)$ during upstroke, with $C \approx 3.5$ is the force coefficient derived empirically[15,35] and C_f is a coefficient chosen, so that the aerodynamic force is 20% greater during downstroke relative to upstroke. This dissymmetry emphasizes the fact that the convex dorsal side of the wing is oriented to the flow during the downstroke, while the concave ventral side of the wing is opposed to the flow during upstroke. The wing camber alteration is due to the stroke reversal of the air circulation around the wing, reducing the effective area of the wing.[16] Therefore, the downstroke force is presumably higher than the upstroke one.

2.4.2. Rotational force. The rotation of the wing about its radial axis deviates the surrounding airflow. The wing reacts to this phenomenon by creating additional rotational circulation[34] and consequently a rotational force modeled by:[31]

$$f_r = \pi \rho l_r C_h^2 \left(\frac{3}{4} - \frac{l_t}{C_h}\right) v^w \dot{\psi} \tag{7}$$

where $\dot{\psi}$ is the first derivative of the rotation angle.

2.4.3. Added mass force. The added mass phenomenon is created by the acceleration of the additional fluid mass surrounding the wing when it accelerates and rotates. It can be modeled by:[31]

$$f_m = \frac{\pi}{4}\rho L l_r C_h^2 \ddot{\phi} \tag{8}$$

where $\ddot{\phi}$ is the second derivative of the flapping angle.

In addition to these forces, the wing is subject to other phenomena like the wake capture, delayed stall, Wagner effect, etc. that have a minor contribution to the total wing lift force and are difficult to model.[34]

The aerodynamic force generated by a wing is applied at its center of pressure, has the direction of the normal vector of the wing $\boldsymbol{n}$. Its expression in the wing's frame $\mathcal{F}^w$ is given by:

$$f^w = f_{qs} + f_r + f_m. \tag{9}$$

The total aerodynamic force $f^b \in \mathbb{R}^3$, generated by the left and right wings, expressed in the body frame $\mathcal{F}^b$ is given by:

$$f^b = R_l^b\, f_l^w + R_r^b\, f_r^w \tag{10}$$

https://doi.org/10.1017/S0263574713000209 Published online by Cambridge University Press

with $R^b_{l,r}$ are the rotation matrices from the left or right wing frames to the body frame.

The aerodynamic torque expressed in the body frame is given by:

$$\tau^b = p^b_l \times f^b_l + p^b_r \times f^b_r \tag{11}$$

with $p^b_{l,r}$ is the position of the left or right wing aerodynamic center in the body frame computed by $p^b_{l,r} = R^b_{l,r} p^w$. It is considered, in the present work, that the aerodynamic and pressure centers coincide.

The left and right wing velocities, expressed in the body frame, are computed by deriving the wing center of pressure positions $v^b_{l,r} = \dot{p}^b_{l,r}$. Their projections in the wing frames are obtained by a simple rotation $v^w_{l,r} = R^{l,r}_b v^b_{l,r}$.

2.5. Body's dynamics

The body can be considered as a whole entity and is modeled as a rigid body, to which are attached two wings. The wing inertia is neglected in the present work because their mass is less than 5% of the body's mass.[35] The effect of the wings' inertia due to the high flapping frequency is considered beyond the scope of this paper. Therefore, the FMAV is modeled as a rigid body subject to aerodynamic forces and torques that generate its movement. It is subject also to viscous and gravitational forces.

The rotational kinematics and dynamics of the FMAV are given by Eqs. (12) and (13). The translational dynamics are not presented here for sake of simplicity. The aerodynamic lift force balances the gravity effect in order to stabilize the FMAV in hovering mode. For more details, readers can refer to previous works.[33]

$$\dot{R} = R\omega^\times, \tag{12}$$

$$\dot{\omega} = J^{-1}(\tau^b - \omega^\times J\omega). \tag{13}$$

$\omega \in \mathbb{R}^3$ is the angular velocity with respect to the mobile frame $\mathcal{F}^b$. $\tau^b \in \mathbb{R}^3$ is the aerodynamic torque vector defined in $\mathcal{F}^b$. $J \in \mathbb{R}^{3\times3}$ is the inertia matrix of the body relative to $\mathcal{F}^b$. R is the rotation matrix from the fixed frame $\mathcal{F}^f$ to the mobile frame $\mathcal{F}^b$. $\omega^\times$ is the skew symmetric matrix associated to the vector ω and related to the cross product $(\times)$ such that $\omega^\times a = \omega \times a$, with $a \in \mathbb{R}^3$.

2.6. Control strategy

Aerodynamic forces are function of the wing angles, their derivatives, and some geometric and aerodynamic parameters. Controlling the orientation of the FMAV amounts from controlling the amplitude or the frequency of the wing angles. Considering that the nature's flapping flyers use generally a fixed characteristic frequency except during instantaneous maneuvers execution,[16,27] the wing angle amplitude control is considered.

On the other hand, the wingbeat frequency adopted in the present work is relatively high (100 Hz). Aerodynamic forces and torques, which are generated at the wingbeat frequency, affect the body's movement only by their average values, computed over a wingbeat period. This is proved based on the averaging theory,[3,22,41] which is a strategy usually used in FMAVs control.[35]

Denote by $u = (\phi^l(t), \phi^r(t), \psi^l(t), \psi^r(t))$ the flapping and rotation angles for left and right wings, $v = (\phi^l_0, \phi^r_0, \psi^l_0, \psi^r_0)$ the amplitudes of these angles in Eq. (1), then $u = v\, f_2(t)$. Denote also by $x = (R, \omega)$ the FMAV's rotational state, the model given by Eqs. (12) and (13) can be written in a compact form as:

$$\dot{x} = f_1(x, u). \tag{14}$$

Let $\bar{x} = (\bar{R}, \bar{\omega})$ denote the averaged state over a wingbeat period T. The compact form of the FMAV's model, averaged over a wingbeat period, is given by:

$$\dot{\bar{x}} = \bar{f}_1(\bar{x}, v). \tag{15}$$

Averaging theory shows that an exponential stable equilibrium state for the averaged dynamics of a high-frequency oscillating system $(\bar{x} = x_e)$ is also a stable equilibrium state for the oscillating (time variant) system, there exists $k > 0$ such that $\|x(t) \otimes \bar{x}(t)\| < kT$ for all $t \in [0, \infty)$, with $\otimes$ designates a comparison operator and T the wingbeat period, which is small in the present case.

As mentioned previously, the FMAV is controlled indirectly by means of the wing angle amplitudes v that will be computed using a feedback $h(\cdot)$ of direct sensors measurements ω and s_k, $k \in \{1, \ldots, n\}$ with n the number of onboard reference sensors

$$v = h(\omega, s_k). \tag{16}$$

Using the inverse reasoning, the control strategy is defined as follows. On the one hand, based on the desired and current orientations, measured by onboard sensors, a control torque is computed. This control is actually equal to the average torque $\bar{\tau}$ over a wingbeat period, $\bar{\tau} = \mathcal{U}(\omega, s_k)$. On the other hand, based on the expression of the aerodynamic torque, a relation between the mean torque $\bar{\tau}$ and the wing angle amplitudes is determined. Recall that the flapping and rotation angle amplitudes (ϕ_0, ψ_0) are the control inputs. Therefore, $\bar{\tau} = \Lambda(\phi_0, \psi_0)$. The inverse relation can be used to compute the wing angle amplitudes that should be applied at the beginning of a wingbeat period, function of the control torque, $(\phi_0, \psi_0) = \Lambda^{-1}(\bar{\tau}) = \Lambda^{-1}(\mathcal{U}(\omega, s_k))$. Therefore, $h(\cdot) = \Lambda^{-1}(\mathcal{U}(\cdot))$.

Two actuators are used for each wing to generate the flapping and rotation angles, creating then the roll and yaw movements of the FMAV. The pitch movement is generated by moving a small mass inside the body using the ElectroWetting On Dielectric (EWOD) technology.[32] A similar strategy using a bobweight actuator inside the FMAV has also been adopted.[28]

Remark 4. Analyzing only the rotational movement of the FMAV, the system can be considered as fully actuated. However, when studying the translational movement, the system will become underactuated and a coupling of the rotational and translational dynamics should be performed

https://doi.org/10.1017/S0263574713000209 Published online by Cambridge University Press

to execute a three-dimensional movement. Hence, arises the importance of the attitude control.

Computing the averaged roll and yaw torques, function of the flapping and rotation angle amplitudes, one has the explicit form of the trigonometric function $\Lambda(\cdot)$:

$$\begin{aligned} \bar{\tau}_1 &= \beta l_r \left[\phi_0^{r^2} \cos \psi_0^r - \phi_0^{l^2} \cos \psi_0^l \right] \\ \bar{\tau}_3 &= \alpha l_r \left[\phi_0^{r^2} \sin \psi_0^r - \phi_0^{l^2} \sin \psi_0^l \right] \end{aligned} \tag{17}$$

with

$$\alpha = \tfrac{2}{T^2} \tfrac{1+(1-2\kappa)C_f}{\kappa(1-\kappa)} \rho C S_w l_r^2,$$
$$\beta = \tfrac{2}{T^2} \tfrac{1-2\kappa+C_f}{\kappa(1-\kappa)} \rho C S_w l_r^2.$$

Each species is characterized by maximum flapping and rotation angles. In a practical point of view, this represents also a technological constraint because the actuators inputs should be bounded to avoid their saturation. Therefore,

$$\begin{aligned} 0 \leq \phi_0 &\leq \phi_{0_{\max}} \\ 0 \leq \psi_0 &\leq \psi_{0_{\max.}} \end{aligned} \tag{18}$$

The roll and yaw torques are therefore bounded. Note also that the movement of the mass inside the body is limited by the body length, the mass and velocity used within the EWOD technology, therefore, the pitch control is bounded too. Resuming, $\bar{\tau} \in [-\tau_{\max}, \tau_{\max}]$.

3. Biologically Inspired Attitude Stabilization

The attitude stabilization problem consists in reaching a desired orientation and maintaining it all over the time. The error between the desired orientation defined by R_d and the current orientation defined by R is denoted by $R_e = RR_d^T$. Therefore, the attitude stability condition is expressed as:

$$\begin{cases} \omega & \to 0 \\ R_e & \to I_3 \end{cases}$$

with I_3 as the three-dimensional identity matrix. The angular velocity can be directly accessed based on the measurements of the rate gyros. However, no measurement of the rotation matrix can be obtained without using estimation strategies. Therefore, a biologically inspired technique is used in this work. It consists on defining the attitude error by means of the FMAV's onboard sensors, which are equivalent to the animal flapping flyers' sensitive organs as it was described earlier. It is actually equal to the error between the onboard sensor measurements and the desired measurements without any computation of the body's orientation. Let s_k^b and s_k^f, $k \in \{1, \ldots, n\}$ denote the measurement of the onboard sensor k in the body frame $\mathcal{F}^b$ and fixed frame $\mathcal{F}^f$, respectively, with n the total number of the embarked reference sensors. The projections of the unit vector $\boldsymbol{s}_k$ in the body and fixed frames are linked through the rotation matrix R such as $s_k^b = Rs_k^f$. Note that s_k^b is called vector observation and s_k^f reference vector. The attitude error γ is defined as:

$$\gamma = \frac{1}{n} \sum_{k=1}^{n} \left(Rs_k^f \right) \times \left(R_d s_k^f \right) = \frac{1}{n} \sum_{k=1}^{n} s_k^b \times R_d s_k^f. \tag{19}$$

Reaching the desired attitude is expressed by a rotation matrix R equal to the desired one R_d, i.e., relative to the accessible information $\gamma = 0$. Reversely, $\gamma = 0$ means that s_k^b and $R_d s_k^f$ are collinear in Eq. (19). Since $\boldsymbol{s}_k$ is a unit vector, then $s_k^b = \pm R_d s_k^f$. Two cases can be identified: (i) $s_k^b = R_d s_k^f$, i.e., the vectors observation has the same orientation of the desired reference vectors direction in $\mathcal{F}^b$, which defines the final goal to reach, and (ii) $s_k^b = -R_d s_k^f$, i.e., the vectors observation has the opposite direction of the desired reference vectors direction in $\mathcal{F}^b$. Therefore, they are defined by a rotation of 180° (π rad) with respect to a plane, axis, or point. The symmetry surface depends actually on the number of reference sensors or more precisely on the number of noncollinear reference vectors n such that $k \in \{1, \ldots, n\}$. Three cases are analyzed:

(a) $n = 1$. If only one vector observation is afforded, it is linked to the reference vector by means of the rotation matrix R as $s_1^b = Rs_1^f$ providing a two-dimensional constraint and unveiling any rotation about the axes s_1^b or s_1^f, in the body and fixed frames, respectively. Therefore, at least two different sensor measurements should be provided instantaneously to have complete information about the attitude error,[25] $n \geq 2$. The case $n = 1$ is, therefore, excluded.

(b) $n = 2$. The symmetry surface is limited to an axis $\boldsymbol{n}$ perpendicular to the plane containing the two vectors $R_d s_k^f$, $k \in \{1, 2\}$, at the vectors intersection. Therefore, $s_k^f = -R_d s_k^f = R_s R_d s_k^f$ with R_s as the rotation matrix defining the symmetry, i.e., the rotation matrix about the axis $\boldsymbol{n}$ of 180°. In the specific case where $R_d s_k^f$ belong to one of the basis planes (e_1^f, e_2^f), (e_1^f, e_3^f), or (e_2^f, e_3^f), then the rotation is performed, respectively, with respect to the axes $\boldsymbol{e}_3^f$, $\boldsymbol{e}_2^f$, and $\boldsymbol{e}_1^f$. These special cases chiefly facilitate the problem and therefore, a choice of the reference sensors should be done this way. This technique is adopted in the present paper. The matrix R_s is given by:

$$R_s \in \{\text{diag}(-1, 1, 1),\ \text{diag}(1, -1, 1),\ \text{diag}(1, 1, -1)\}. \tag{20}$$

(c) $n \geq 3$. $s_k^b = -R_d s_k^f = SR_d s_k^f$ where S is the reflexion matrix defined by diag$(-1, -1, -1)$. Note that S is not a rotation matrix because $\det S = -1$ and $\operatorname{Tr} S = -3$. No rotation matrix can therefore be identified and the configuration $s_k^b = -R_d s_k^f$ cannot be reached.

Resuming, the set of couples (ω, R) for which the attitude stability is reached, $(\omega = 0,\ \gamma = 0)$, is given by:

$$\mathcal{E} = \{(\omega, R) \in TSO(3) : \omega = 0,\ R = \mathcal{P} R_d\} \tag{21}$$

https://doi.org/10.1017/S0263574713000209 Published online by Cambridge University Press

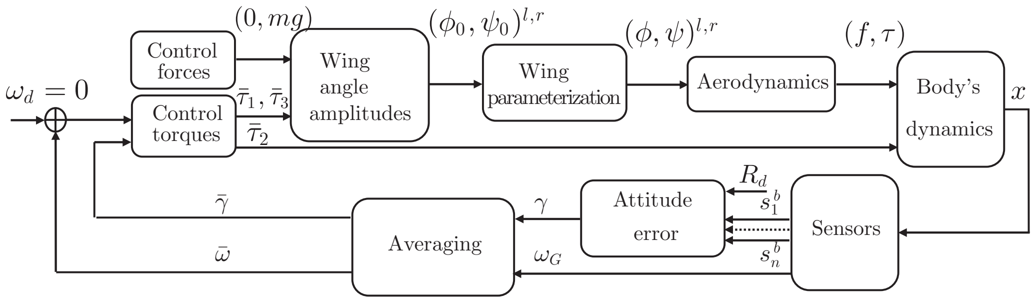

Fig. 4. The block diagram of the FMAV's attitude control based on sensors measurements.

with

$$\mathcal{P} = \{\mathrm{diag}(1, 1, 1),\ \mathrm{diag}(-1, 1, 1),\ \mathrm{diag}(1, -1, 1),\ \mathrm{diag}(1, 1, -1)\}. \tag{22}$$

The block diagram of the closed-loop attitude control is given in Fig. 4, where the different blocks have been defined previously. In the following, the control torques will be addressed. The control forces are set such that they balance the gravity and ensure no movement along the three axes of the fixed frame $\mathcal{F}^f$.

3.1. Bounded attitude control

A bounded control torque computed using the direct measurements of onboard sensors is proposed. This control takes into consideration the saturation of the actuators and is simple to implement. First, the asymptotical stability of the rigid body is shown, then the proof is extended to show the stability of the FMAV. It is assumed that there exist at least two non-collinear vector observations embarked on the FMAV such that $n \geq 2$.

Proposition 1. Consider the FMAV's rotational dynamics described by Eqs. (12) and (13). The attitude error γ between the current and desired body's orientations is defined by Eq. (19) with $n \geq 2$. The FMAV body's angular velocity $\omega = [\omega_1, \omega_2, \omega_3]^T$ is measured by three rate gyros. Define the bounded control $\bar{\tau} = [\bar{\tau}_1, \bar{\tau}_2, \bar{\tau}_3]^T$ by:

$$\bar{\tau}_j = -\mathrm{sat}_{N_j}\left(\frac{\lambda \bar{\omega}_j}{\rho_j} + \lambda \bar{\gamma}_j\right), \qquad j \in \{1, 2, 3\} \tag{23}$$

with $\bar{\omega}, \bar{\gamma}$ are, respectively, the averaged angular velocity and attitude error computed over a wingbeat period T, N_j is the bound of the control torque component $\bar{\tau}_j$, $\mathrm{sat}_{N_j}(\cdot)$ is a classical saturation function, λ is a positive real parameter such that $0 < \lambda \leq \min(N_j/2)$ and ρ_j, $j \in \{1, 2, 3\}$ are positive scaling parameters. The control torque in Eq. (23) stabilizes the FMAV at $(\omega, R) = (0, R_d)$ with a domain of attraction equal to $T\mathrm{SO}(3) \setminus \{(0, R_s R_d)\}$, R_s is given in Eq. (20).

Proof. Lets first prove the stability of a rigid body whose state vector is the averaged state vector of an FMAV. The dynamics of the rigid body are then given by Eqs. (12) and (13) where the angular velocity is denoted by $\bar{\omega}$, the rotation matrix by $\bar{R}$, the control torque by $\bar{\tau}$, and the attitude error by $\bar{\gamma}$. Note that the derivative of an averaged vector observation $\bar{s}_k^b$ is linked to the vector by means of

$$\dot{\bar{s}}_k^b = \bar{s}_k^b \times \bar{\omega} = -\bar{\omega} \times \bar{s}_k^b. \tag{24}$$

Note also that the reference vectors are well known and fixed vectors; the average, over a wingbeat period, is equal to the vector.

Consider first the following definite positive Lyapunov function:

$$V = \frac{1}{2}\bar{\omega}^T J \bar{\omega}, \tag{25}$$

where J is the inertia matrix of the body. V is trivially positive definite and radially unbounded. The derivative of Eq. (25) along the trajectories of the closed-loop system is given by:

$$\dot{V} = \bar{\omega}^T J \dot{\bar{\omega}} = \underbrace{\bar{\omega}^T(-\bar{\omega}^\times J \bar{\omega})}_{=0} + \bar{\omega}^T \bar{\tau} = \bar{\omega}^T \bar{\tau} = \sum_{j=1}^{3} \bar{\omega}_j \bar{\tau}_j. \tag{26}$$

One gets from $\bar{\tau}_j$ in Eqs. (23) and (26) that

$$\dot{V} = -\sum_{j=1}^{3} \bar{\omega}_j \mathrm{sat}_{N_j}\left(\frac{\lambda \bar{\omega}_j}{\rho_j} + \lambda \bar{\gamma}_j\right).$$

Let $\Phi = \{\bar{\omega} : |\bar{\omega}| \leq \rho + \varepsilon\}$ for some $\varepsilon > 0$ and $\rho = [\rho_1, \rho_2, \rho_3]^T$. Outside Φ, i.e., $|\bar{\omega}_j| > \rho_j + \varepsilon$, using the unitary condition $|\gamma_j| \leq 1$, it follows that $|\lambda \frac{\bar{\omega}_j}{\rho_j} + \lambda \bar{\gamma}_j| \geq \lambda \frac{\varepsilon}{\rho_j}$ and that $\lambda \frac{\bar{\omega}_j}{\rho_j} + \lambda \bar{\gamma}_j$ and $\bar{\omega}_j$ have the same sign. Therefore,

$$\dot{V} = -\sum_{j=1}^{3} \bar{\omega}_j \mathrm{sat}_{N_j}\left(\frac{\lambda \bar{\omega}_j}{\rho_j} + \lambda \bar{\gamma}_j\right) \leq -\sum_{j=1}^{3} \frac{\lambda \varepsilon}{\rho_j} |\bar{\omega}_j|$$
$$< -\sum_{j=1}^{3} \frac{\lambda \varepsilon(\rho_j + \varepsilon)}{\rho_j} < -3\lambda\varepsilon < 0.$$

Consequently, $\bar{\omega}$ enters in Φ. During this time, $\bar{\gamma}_j$ cannot diverge since it is structurally unitary and therefore bounded. Once in Φ, one has:

$$\left|\frac{\lambda \bar{\omega}_j}{\rho_j} + \lambda \bar{\gamma}_j\right| \leq 2\lambda + \frac{\lambda \varepsilon}{\rho_j}.$$

https://doi.org/10.1017/S0263574713000209 Published online by Cambridge University Press

Taking ε sufficiently small and using the assumption that $2\lambda < N_j$, then:

$$\left|\frac{\lambda\bar{\omega}_j}{\rho_j} + \lambda\bar{\gamma}_j\right| \leq N_j.$$

Consequently, sat_{N_j} operates in a linear region, and the control torque becomes:

$$\bar{\tau}_j = \frac{\lambda}{\rho_j}\left(\bar{\omega}_j + \rho_j\bar{\gamma}_j\right). \quad (27)$$

In Φ, consider the Lyapunov function W defined by:

$$W = \frac{1}{2}\bar{\omega}^T J\bar{\omega} + \frac{\lambda}{n}\sum_{k=1}^{n}\left[1 - \left(\bar{R}s_k^f\right)\left(R_d s_k^f\right)\right], \quad (28)$$

where W is a continuous and positive definite function on TSO(3) because $W > 0$ and $W(0, Rd) = 0$. Since $\bar{s}_k^b = \bar{R}s_k^f$ and s_k^f is constant, the derivative of Eq. (28) is given by:

$$\dot{W} = \bar{\omega}^T J\dot{\bar{\omega}} - \frac{\lambda}{n}\sum_{k=1}^{n}\left(\dot{\bar{s}}_k^b R_d s_k^f\right). \quad (29)$$

By means of Eqs. (19) and (24) and the fact that $\bar{\omega}^T(-\bar{\omega}^\times J\bar{\omega}) = 0$, Eq. (29) becomes:

$$\begin{aligned}\dot{W} &= \bar{\omega}^T\bar{\tau} + \frac{\lambda}{n}\sum_{k=1}^{n}\bar{\omega}^T\left(\bar{s}_k^b \times R_d s_k^f\right)\\ &= \bar{\omega}^T\bar{\tau} + \lambda\bar{\omega}^T\bar{\gamma}\\ &= \sum_{j=1}^{3}(\bar{\omega}_j\bar{\tau}_j + \lambda\bar{\omega}_j\bar{\gamma}_j) = \sum_{j=1}^{3}\dot{W}_j. \end{aligned} \quad (30)$$

Analyzing $\dot{W}_j$ for $j \in \{1, 2, 3\}$, one gets from $\bar{\tau}_j$ in Eqs. (27) and (30) that:

$$\begin{aligned}\dot{W}_j &= -\bar{\omega}_j\left(\frac{\lambda\bar{\omega}_j}{\rho_j} + \lambda\bar{\gamma}_j\right) + \lambda\bar{\omega}_j\bar{\gamma}_j\\ &= -\frac{\lambda}{\rho_j}\bar{\omega}_j^2\end{aligned}$$

and

$$\dot{W} = \sum_{j=1}^{3}\dot{W}_j = -\lambda\sum_{j=1}^{3}\frac{\bar{\omega}_j^2}{\rho_j} \leq 0. \quad (31)$$

The derivative of the Lyapunov function W is negative semidefinite. Recall that TSO(3) is compact. Therefore, for any initial condition $(\bar{\omega}(0), \bar{R}(0)) \in TSO(3)$, the set:

$$\Omega = \{(\bar{\omega}, \bar{R}) \in TSO(3) : W(\bar{\omega}, \bar{R}) \leq W(\bar{\omega}(0), \bar{R}(0))\}$$

is a compact, positively invariant set of the closed-loop. From LaSalle Invariance Principle, it follows that all solutions that start in Ω converge to the largest invariant subset of $\bar{\Omega}$ belonging to Ω. $\dot{W}(\bar{\omega}, \bar{R}) \equiv 0$ implies $\bar{\omega} \equiv 0$, then, substituting this last identity into the closed-loop system in Eqs. (12), (13), and (23), one has

$$\bar{\Omega} = \{(\bar{\omega}, \bar{R}) \in TSO(3) : \bar{\omega} \equiv 0, \bar{\gamma} \equiv 0\}$$

with $\bar{\gamma}$ defined in Eq. (19) over the averaged measurements. Then, the largest invariant subset of $\bar{\Omega}$ is given by $\mathcal{E}$ in Eqs. (21) and (22).

Therefore, $\mathcal{E}$ defines the set of equilibrium points for which the Lyapunov function W in Eq. (28) represents a minimum ($W = 0$) and a local maximum ($W = 2\lambda$) corresponding, respectively, to the rotation matrices $\bar{R} = R_d$ and $\bar{R} = R_s R_d$ with R_s given in Eq. (20). If the system is at one of these points at $t_0 = 0$, it will remain there for all $t \geq t_0$. The control law acts then to ensure the convergence of the closed-loop solutions, whose initial conditions do not verify $(\bar{\omega}, \bar{R}) = (0, R_s R_d)$, to the stable equilibrium point given by $(\bar{\omega}, \bar{R}) = (0, R_d)$ and corresponding to $W = \dot{W} = 0$.

Therefore, the rigid body is asymptotically stable with a domain of attraction equal to $TSO(3) \setminus \{(0, R_s R_d)\}$.

Once the asymptotic stability of the rigid body proven, the stability of the FMAV subject to the control torque in Eq. (23) and computed over the averaged dynamics of the system $(\bar{\omega}, \bar{R})$ will be presented. For that, the averaging theory recalled in Section 2.6 is used. It states that for a high-frequency oscillating system, the averaged and time varying dynamics are very close and therefore, a stable equilibrium of the averaged dynamics is also a stable equilibrium of the time-varying dynamics: $\|\omega - \bar{\omega}\| < k_1 T$ and $\|R\bar{R}^T\| < k_2 T$ for $k_{1,2} > 0$ and T is the wingbeat period. In other words, the state vector (ω, R) of the FMAV, subject to the control torque in Eq. (23), converges to the equilibrium point $(0, R_d)$ with a domain of attraction equal to $TSO(3) \setminus \{(0, R_s R_d)\}$. □

4. Simulations and Robustness Tests

Two strategies have been adopted in the literature to test the control laws developed for animal flapping flyers. The first is based on models of the flapping flight including aerodynamics, body and wing dynamics.[10,12,29,31] Note that well-developed models of flapping flight do not exist because the aerodynamics at low Reynolds numbers have not been yet perfectly identified.[16] The second strategy consists on testing the control in real time on a prototype[19,30] where simple models are proposed and identified. One should emphasize that at microscopic scale, only the vertical movement has been performed on a flapping flyer prototype[30] where the pitch movement is avoided by attaching the FMAV using some wires, the laser sensor measuring the vertical altitude is external as well as the power system. Vertical movement control of a 101 mg FMAV has been also presented.[17] Note that very challenging mass and size of FMAVs can be reached nowadays with the progress of microelectronics. The onboard electronic circuit developed within the OVMI/EVA project weighs 100 mg and is composed of a microprocessor, inertial and optic flow sensors. Piezoelectric actuators can reach 10 mg and are used within FMAVs.[39] Other low size and

https://doi.org/10.1017/S0263574713000209 Published online by Cambridge University Press

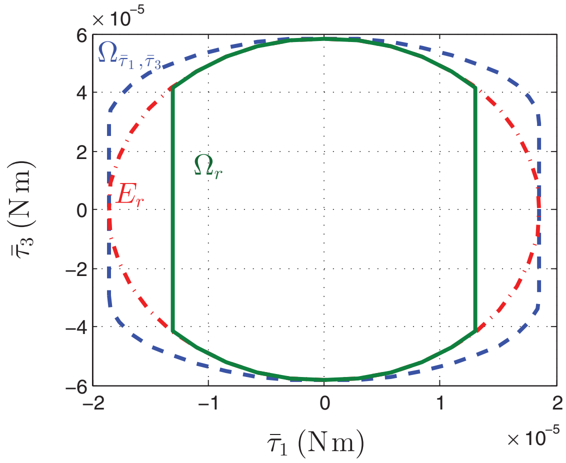

Fig. 5. (Colour online) Yaw torque versus roll torque, defining the saturation set $\Omega_{\bar{\tau}_1,\bar{\tau}_3}$ approximated to an ellipse E_r, then to a set Ω_r.

weight microelectronic devices exist on the market for such applications. The power supply remains very difficult to embark.

In the present work, the first strategy is adopted. For simulations, the physical data of a dipteran insect are used.[16] The mass is of 200 mg and the wingbeat frequency of 100 Hz. The maximum amplitudes for flapping and rotation angles are taken to $\phi_{0_{\max}} = 60^\circ$ and $\psi_{0_{\max}} = 90^\circ$, respectively. The wingspan and wings surface are assumed, respectively, to $2\,L = 3\,\text{cm}$ and $2\,S_w = 1.14\,\text{cm}^2$, allowing to generate a vertical ascendant movement using admissible flapping angles amplitudes.

Based on the defined numerical values, the admissible set for control torques $\Omega_{\bar{\tau}_1,\bar{\tau}_3}$ can be determined in Eq. (17) and plotted (Fig. 5).

$\Omega_{\bar{\tau}_1,\bar{\tau}_3}$ is approximated to the largest ellipse E_r that fits inside $\Omega_{\bar{\tau}_1,\bar{\tau}_3}$ (Fig. 5) for computation simplification reasons.

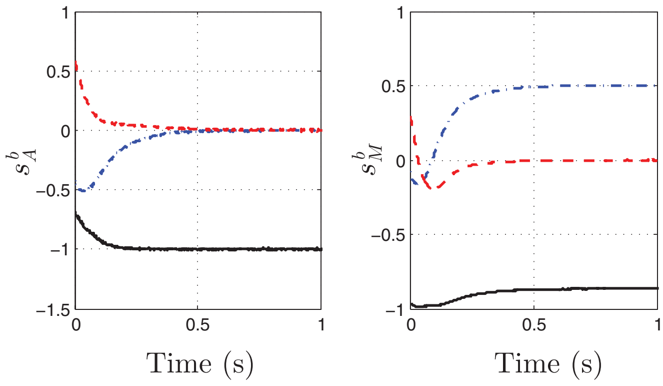

Fig. 7. (Colour online) The reference sensor measurements: accelerometer (left) and magnetometer (right). The measurement along the roll axis is plotted with dot-dashed blue line, the pitch axis with dashed red line, and yaw axis with continuous black line.

The control torques $\bar{\tau}_1$ and $\bar{\tau}_3$ respect then an ellipsoidal admissible set defined by

$$[\bar{\tau}_1\ \bar{\tau}_3]Q[\bar{\tau}_1\ \bar{\tau}_3]^T \leq 1, \tag{32}$$

where Q is a diagonal definite positive matrix defining the ellipse's semi-axes denoted by a_r and b_r. Practically, if $\bar{\tau}_1 \geq a_r$ in Eq. (23), $\bar{\tau}_1$ could be saturated to a_r, and $\bar{\tau}_3$ will be equal to zero. A privilege is given to the roll control in order to bring the FMAV to the horizontal plane. To avoid having a null yaw control torque and to give preference to the roll movement, 70% of a_r is attributed to N_1, $\bar{\tau}_3$ will be calculated by Eq. (32) defining then a set Ω_r (Fig. 5).

The control torque in Eq. (23) is applied to the FMAV to be validated in simulation. Three sensors are embarked on the FMAV to mimic a part of the sensory system of an insect (halteres, legs sensilla, and magnetic sense): three rate gyros, a tri-axis accelerometer, and a tri-axis magnetometer whose

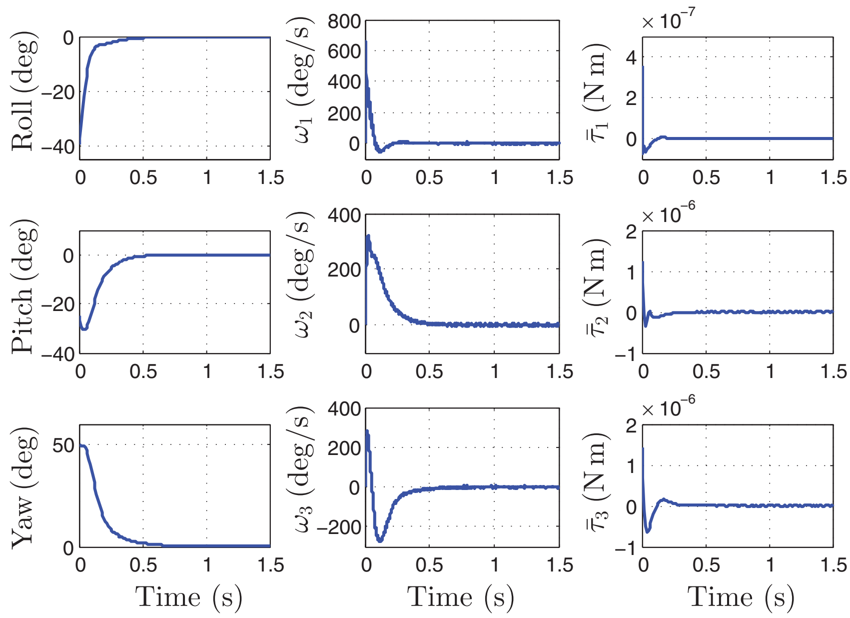

Fig. 6. (Colour online) The attitude (left), angular velocity (middle) of the FMAV going from initial roll, pitch, and yaw angles $(-40^\circ, -25^\circ, 50^\circ)$ and null angular velocity, and the control torques (right) applied to the FMAV.

https://doi.org/10.1017/S0263574713000209 Published online by Cambridge University Press

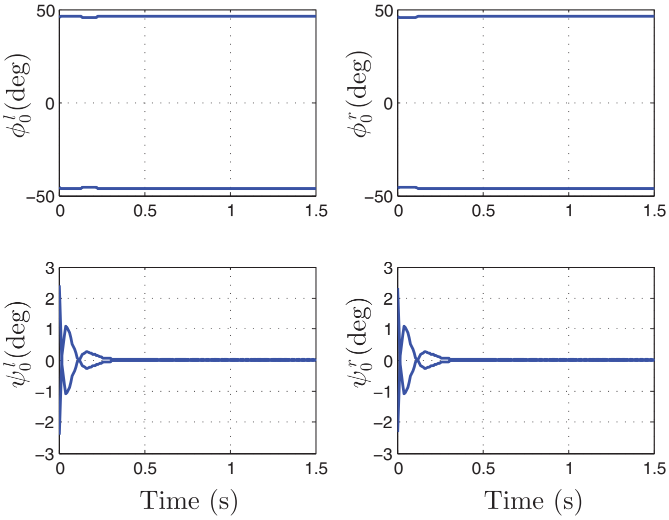

Fig. 8. (Colour online) The envelops of the left and right wing angles.

models are given by Eqs. (3)–(5), respectively. The sensors measurements are not perfect, additive white Gaussian noise is considered having a standard deviation of $\sigma_G = 10^{-3}$ rad/s for the rate gyros, $\sigma_A = 10^{-4}$ m/s^2 for the accelerometer, and $\sigma_M = 0.01$ mGauss for the magnetometer. Because of the low inertia of the FMAV, the developed control torque has also very small values of almost 10^{-5} N m (Fig. 5). Since the control law is computed through a feedback of direct sensor measurements, the sensors should have a remarkable precision in order to guarantee a reasonable signal-to-noise ratio. Note that sensors with suitable precision or sensibility have already been developed.[8] Even if the averaging of the angular velocity and attitude error reduces the noise influence, it cannot be totally eliminated. The tuning parameters considered in simulations are given by $(N_1, N_2, N_3) = (0.7\,a_r, 10^{-5}, \frac{b_r}{a_r}\sqrt{a_r^2 - \bar{\tau}_1^2})$ with $(a_r, b_r) = (1.859 \times 10^{-5}, 5.843 \times 10^{-5})$, $\lambda = 5 \times 10^{-6}$, $(\rho_1, \rho_2, \rho_3) = (\frac{2.2\times 10^{-3}}{a_r}, 15.5, \frac{5\times 10^{-4} a_r}{b_r\sqrt{a_r^2-\bar{\tau}_1^2}})$.

The evolution of the roll, pitch, and yaw angles as well as the angular velocities measured by the rate gyros and the control torques are plotted in Fig. 6. Note that the body's angles are not used in the control torque, they are plotted only to show the convergence of the FMAV's orientation. The initial orientation is $(-40^\circ, -25^\circ, 50^\circ)$ for the roll, pitch, and yaw angles, respectively. The initial angular velocity is null. The sensor measurements are presented in Fig. 7 and the wing angle amplitude envelops in Fig. 8. The stability is reached in a sufficiently fast time that makes the control law suitable for real-time implementation on an FMAV. Moreover, it presents comparable values to those observed in true insects.[16] The rate gyros noise is detectable in Fig. 6. The accelerometer's noise is more detectable than that of the magnetometer. Their measurements converge to $s_A^f = [0, 0, -1]^T$ and $s_M^f = [\frac{1}{2}, 0, -\frac{\sqrt{3}}{2}]$ at the equilibrium. Recall that the FMAV is stabilized in hovering mode. Therefore, the flapping angles converge to the value that generates an aerodynamic lift balancing its weight. The rotation angles converge to zero, so that no translational movement is generated.

The robustness of the control law is tested with respect to external disturbances. These disturbances simulate wind or rain drops affecting the FMAV and creating a body torque of $(1.2 \times 10^{-5}, 2 \times 10^{-5}, 1.2 \times 10^{-5})$ N m, applied at $t = 1.5$ s during 10 wingbeat periods. Noting that a rain drop weighs about 5×10^{-6} N and the FMAV body's inertia is of 10^{-8} kg m^2, the disturbance applied has a great effect on the body's movement. It will destabilize the FMAV all over the disturbance taking it far away from the equilibrium. The control law acts later on to bring the FMAV back to the stability. The evolution of the roll, pitch, and yaw

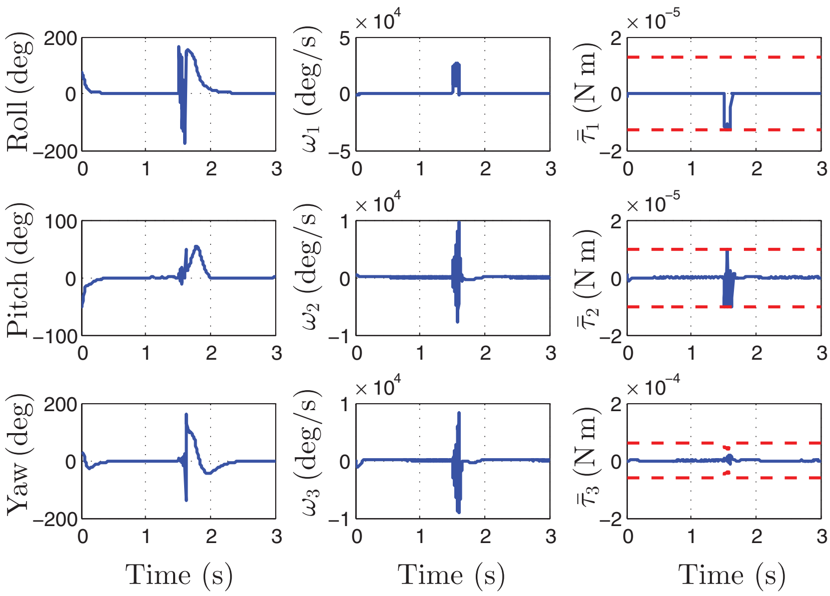

Fig. 9. (Colour online) Robustness with respect to external disturbances: the attitude (left), angular velocity (middle), and the control torques (right) applied to the FMAV.

https://doi.org/10.1017/S0263574713000209 Published online by Cambridge University Press

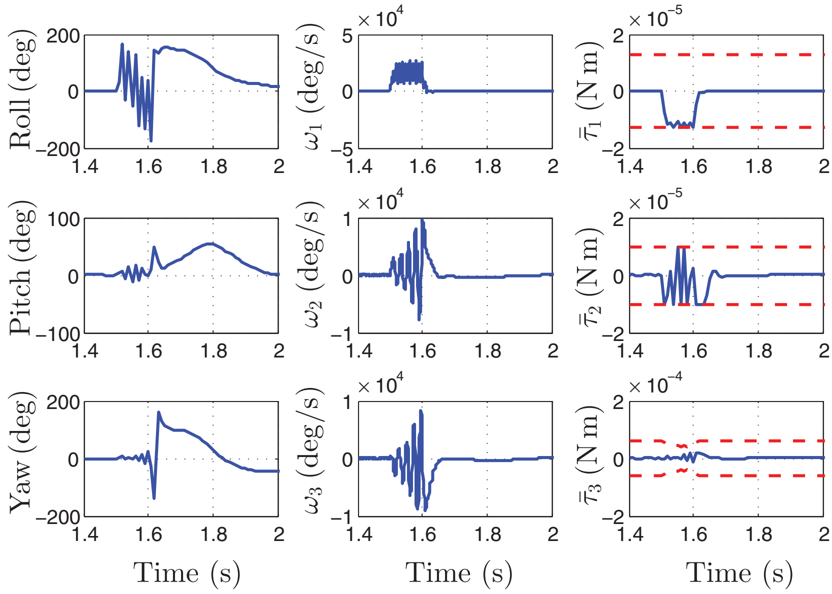

Fig. 10. (Colour online) Robustness with respect to external disturbances: the attitude (left), angular velocity (middle), and the control torques (right) applied to the FMAV zoomed to the disturbance.

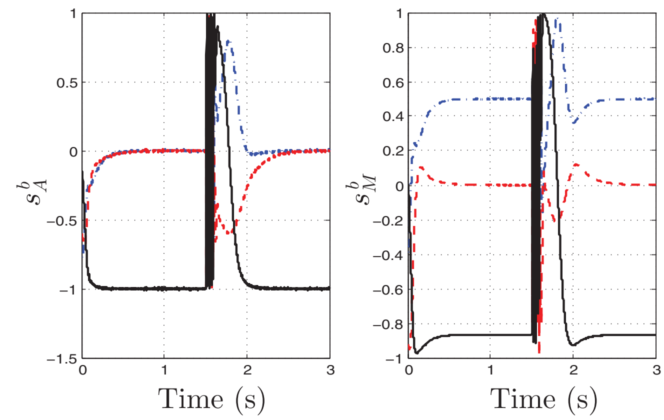

Fig. 11. (Colour online) Robustness with respect to external disturbances: the reference sensor measurements: accelerometer (left) and magnetometer (right). The measurement along the roll axis is plotted with dot-dashed blue line, the pitch axis with dashed red line, and yaw axis with continuous black line.

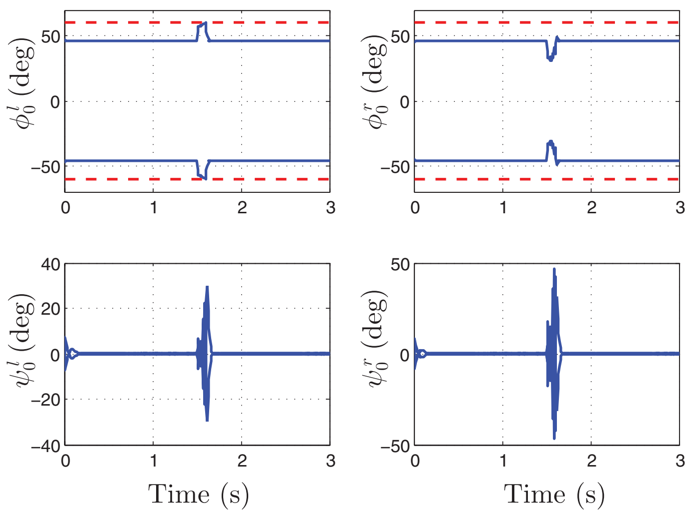

Fig. 12. (Colour online) Robustness with respect to external disturbances: the envelops of the left and right wing angles. The bounds of the flapping angles are plotted with red-dashed lines.

angles, angular velocities, and control torques is plotted in Fig. 9, zoomed to the disturbance zone in Fig. 10. Note that the bound of the yaw torque depends on the value of the roll torque as explained previously. The reference sensor measurements are given in Fig. 11 and the wing angle amplitudes in Fig. 12. Notice that the flapping angle of the left wing is bounded during the disturbance at $\phi_{\max} = 60^\circ$ avoiding the saturation of the actuator and emphasizing the development of a bounded control law. One should also note that an insect subject to such a high disturbance will lose all control of its position and orientation and regain it only when the disturbance is over.

5. Conclusions and Future Works

Even if the gap between the flapping-wing animal flight and its technological reproduction is still very large, the robotic and control communities are exerting big effort to develop FMAVs that mimic the nature's flight the most accurately possible.

The main contribution of this work is the development of a control law stabilizing the FMAV's attitude. It is based directly on the measurements of some embedded sensors without the need of computing the orientation. This strategy reproduces the insects technique of stabilizing their orientation, based on their halteres, legs sensilla and magnetic sense. The control torque is bounded, allowing to take into account the amplitude bounds of the flapping wings in order to avoid the saturation of the actuators and ensure the stability of the body. Note that it allows different saturation bounds along the three axes. It is also not restricted to symmetric bodies and independent of the inertia matrix. Moreover, it is simple to compute and is adaptable

https://doi.org/10.1017/S0263574713000209 Published online by Cambridge University Press

for real-time implementation. As shown in simulations, the control law is robust with respect to external disturbances. The boundedness of the control torque helps preserving the piezoelectric actuators not saturated and guarantees then their linear behavior even in hard conditions.

Future works will consider the development of bounded control force aiming to control the FMAV's trajectory based on sensor's measurements. In fact, insects can determine the Sun direction using their ocelli. Moreover, the light polarization direction can be determined using the compound eyes. Based on polarized light compasses, for example, one can determine the direction of flight and couple it with the attitude control in order to ensure a movement in the three-dimensional space.

References

1. D. E. Alexander, "Wind tunnel studies of turns by flying dragonflies," *J. Exp. Biol.* **122**, 81–98 (1986).
2. D. E. Alexander and S. Vogel, *Nature's Flyers: Birds, Insects and the Biomechanics of Flight* (Johns Hopkins University Press, Baltimore, 2004).
3. F. Bullo, "Averaging and vibrational control of mechanical systems," *SIAM J. Control Optim.* **41**(2), 452–562 (2002).
4. D. Campolo, G. Barbera, L. Schenato, L. Pi, X. Deng and E. Guglielmelli, "Attitude stabilization of a biologically inspired robotic housefly via dynamic multimodal attitude estimation," *Adv. Robot.* **23**(7–8), 955–977 (2009).
5. D. Campolo, M. Sitti and R. S. Fearing, "Efficient charge recovery method for driving piezoelectric actuators with quasi-square waves," *IEEE Trans. Ultrason. Ferroelectr. Freq. Control* **50**(3), 237–244 (2003).
6. R. Chapman, "*The Insects: Structure and Function*, 4th ed. (Cambridge University Press, Cambridge, 1998).
7. M. Epstein, S. Waydo, S.-B. Fuller, W. Dickson, A. Straw, M.-H. Dickinson, and R.-M. Murray. Biologically inspired feedback design for drosophila flight. In *American Control Conference*, New York, USA (2007) pp. 3395–3401.
8. P. Cheinet, B. Canuel, F. Pareira Dos Santos, A. Gauguet, F. Leduc and A. Landragin, "Measurement of the sensitivity function in time-domain atomic interferometer," *IEEE Trans. Instrum. Meas.* **57**(6), 1141–1148 (2008).
9. S.-J. Chung and M. Dorothy, "Neurobiologically inspired control of engineered flapping flight," *J. Guid. Control Dyn.* **33**(2), 440–453 (2010).
10. M.-S. Couceiro, J.-M. Luz, C.-M. Figueiredo and N.-M. Fonseca Ferreira, "Modeling and control of biologically inspired flying robots," *Robotica* **30**(1), 107–121 (2012).
11. X. Deng, L. Schenato and S. Sastry, "Model Identification and Attitude Control for a Micromechanical Flying Insect Including Thorax and Sensor Models," *Proceedings of the IEEE International Conference on Robotics and Automation*, Taipei, Taiwan (2003) pp. 1152–1157.
12. X. Deng, L. Schenato, W.-C. Wu and S. Sastry, "Flapping flight for biomimetic robotic insects: Part I system modeling," *IEEE Trans. Robotics* **22**(4), 776–788 (2006a).
13. W. Shyy, H. Aono, S.-K. Chimakurthi, P. Trizila, C.-K. Kang, C.E. Cesnik and H. Liu. Recent progress in flapping wing aerodynamics and aeroelasticity. *Progress in Aerospace Sciences*, **46**(7), 284–327 (2010).
14. X. Deng, L. Schenato, W.-C. Wu and S. Sastry, "Flapping flight for biomimetic robotic insects: Part II flight control design," *IEEE Trans. Robotics* **22**(4), 789–803 (2006b).
15. M. Dickinson, F.-O. Lehmann and S. Sane, "Wing rotation and the aerodynamic basis of insect flight," *Science* **284**(5422), 1954–1960 (1999).
16. R. Dudley, *The Biomechanics of Insect Flight: Form, Function, Evolution* (Princeton Univesity Press, Princeton, 2002).
17. P.-E. Duhamel, N.-O. Pérez-Arancibia, G.-L. Barrows and R.-J. Wood, "Altitude Feedback Control of a Flapping-Wing Microrobot Using an On-Board Biologically Inspired Optical Flow Sensor," *Proceedings of the IEEE International Conference on Robotics and Automation*, St Paul, MN, USA (2012) pp. 4228–4235.
18. B.-M. Finio, B. Eum, C. Oland and R.-J. Wood, "Asymmetric Flapping for a Robotic Fly Using a Hybrid Power-Control Actuator," *Proceedings of the International Conference on Intelligent Robots and Systems*, St. Louis, MO, USA (2009) pp. 2755–2762.
19. B.-M. Finio, N.-O. Pérez-Arancibia and R.-J. Wood, "System Identification and Linear Time-Invariant Modeling of an Insect-Sized Flapping-Wing Micro Air Vehicle," *Proceedings of the International Conference on Intelligent Robots and Systems*, San Francisco, CA, USA (2011) pp. 1107–1114.
20. T. Hedrick and T. Daniel, "Flight control in the hawkmoth Manduca sexta: the inverse problem of hovering," *J. Exp. Biol.* **209**(16), 3114–3130 (2006).
21. H. Janocha and C. Stiebel, "New Approach to a Switching Amplifier for Piezoelectric Actuators," *Proceedings of the 6th International Conference on New Actuators*, Bremen, Germany (1998) pp. 189–192.
22. H. Khalil, *Nonlinear Systems* (Prentice Hall, Upper Saddle River, NJ, 2002).
23. K. Kuhnen, H. Janocha, D. Thull and A. Kugi, "A New Drive Concept for High-Speed Positioning of Piezoelectric Actuators," *Proceedings of the 10th International Conference on New Actuators*, Bremen, Germany (2006) pp. 82–85.
24. D. Lentink and A.-A. Biewener, "Nature-inspired flight – beyond the leap," *Bioinspiration and Biomimetics* **5**(4), 040201 (2010).
25. F. L. Markley, J. L. Crassidis and Y. Cheng, "Nonlinear Attitude Filtering Methods," *AIAA Guidance, Navigation, and Control Conference*, San Fancisco, California (2005) paper no. 5927.
26. A.-M. Mountcastle and T.-L. Danie, "Vortexlet models of flapping flexible wings show tuning for force production and control," *Bioinspiration and Biomimetics* **5**(4), 045005 (2010).
27. W. Nachtigall and D.-M. Wilson, "Neuro-muscular control of dipteran flight," *J. Exp. Biol.* **47**, 77–97 (1967).
28. M.-W. Oppenheimer, D.-B. Doman and D.-O. Sightorsson,"Dynamics and Control of a Minimally Actuated Biomimetic Vehicle: Part II Control," *Proceedings of the AIAA Guidance, Navigation and Control Conference*, Chicago, Illinois, USA (2009) p. 6161.
29. M.-W. Oppenheimer, D.-B. Doman and D.-O. Sightorsson, "Dynamics and Control of a Biomimetic Vehicle Using Biased Wingbeat Forcing Functions: Part I Aerodynamic Model," *Proceedings of the 48th AIAA Aerospace Sciences Meeting*, Orlando, Florida, USA (2010) p. 1023.
30. N.-O. Perez-Arancibia, K.-Y. Ma, K.-C. Galloway, J.-D. Greenberg and R.-J. Wood, "First controlled vertical flight of a biologically inspired microrobot," *Bioinspiration and Biomimetics* **6**(3), 036009 (2011).
31. T. Rakotomamonjy, M. Ouladsine and T. LeMoing, "Longitudinal modelling and control of a flapping-wing micro aerial vehicle," *Control Engineering Practice* **18**(7), 679–690 (2010).
32. A. Renaudin, V. Zhang, P. Tabourier, J. Camart and C. Druon, "Droplet Manipulation Using SAW Actuation for Integrated Microfluidics," *μTAS*, Malmö, Sweden (2004) pp. 551–553.
33. H. Rifai, N. Marchand and G. Poulin, "Bounded Control of a Flapping Wing Micro Drone in Three Dimensions," *Proceedings of the 2008 IEEE International Conference on Robotics and Automation*, Pasadena, California, USA (2008) pp. 164–169.
34. S. Sane, "Review the aerodynamics of insect flight," *J. Exp. Biol.* **206**(23), 4191–4208 (2003).
35. L. Schenato, D. Campolo and S. Sastry, "Controllability Issues in Flapping Flight for Biomimetic Micro Aerial Vehicles (MAVs)," *International Conference on Decision and Control* Maui, Hawaii, USA (2003) pp. 6441–6447.

36. L. Schenato, W.-C. Wu and S. Sastry, "Attitude control for a micromechanical flying insect via sensor output feedback," *IEEE Trans. Robot. Autom.* **20**(1), 93–106 (2004).
37. K. Senda, M. Sawamoto, M. Kitamura and T. Obara, "Effects of Flexibly Torsional Wings in Flapping-of-Wings Flight of Butterfly," *World Automation Congress*, Hawaii, USA (2008) pp. 1–6.
38. P.-S. Sreetharan and R.-J. Wood, "Passive torque regulation in an underactuated flapping wing robotic insect," *Auton. Robots* **31**(2–3), 225–234 (2011).
39. E. Steltz and R.-S. Fearing, "Dynamometer Power Output Measurements of Piezoelectric Actuators," *Proceedings of the International Conference on Intelligent Robots and Systems*, San Diego, California, USA (2007) pp. 3980–3986.
40. S.-L. Thomson, C.-A. Mattson, M.-B. Colton, S.-P. Harston, D.-C. Carlson and M. Cutler, "Experiment-Based Optimization of Flapping Wing Kinematics," *Proceedings of the 47th AIAA Aerospace Sciences Meeting*, Orlando, Florida (2009) p. 874.
41. P. A. Vela, Averaging and Control of Nonlinear Systems, *Ph.D. Thesis*, (California: California Institute of Technology, 2003).

https://doi.org/10.1017/S0263574713000209 Published online by Cambridge University Press